Characterization of Poly(p-phenylene-cis-benzobisoxazole) in Methanesulfonic Acid

D. B. Roitman,*,† R. A. Wessling, and J. McAlister

Central Research and Development, The Dow Chemical Company, 2800 Mitchell Drive, Walnut Creek, California 94598

Received March 1, 1993; Revised Manuscript Received June 30, 1993®

ABSTRACT: Poly(p-phenylene-cis-benzobisoxazole) (cis-PBO) articles such as fibers possess exceptional mechanical strengths and moduli as well as high thermal performance and chemical resistance. These properties are assumed to be the result of the "rodlike" shape of this polymer. The intrinsic viscosity dependence on molecular weight (Mark-Houwink relationship) and the dependence of radius of gyration R_g with the degree of polymerization in methanesulfonic acid (MSA) solutions, however, suggest considerable deviations from rodlike behavior. This behavior might be attributed either to aggregation or to a semistiff backbone. A polyelectrolyte semistiff chain model was in excellent agreement with the light scattering and viscometric experimental results. The apparent chain flexibility of cis-PBO in solution was attributed to a significant "kidney-bean" shape of the heterocycles induced by the protonation of the N-atoms. The uncharged chain on the other hand, appears to conform more closely than the chain in solution to the ideal rodlike model.

Introduction

The PBZ-type heterocyclic aromatic polymers are a family of high-performance materials with excellent chemical and thermal stability.[1] These polymers form lyotropic liquid crystalline solutions[2,3] and can be spun into fibers with exceptionally high tensile moduli and strengths.

The most widely studied PBZs are[1-8] poly(p-phenylene-cis-benzobisoxazole) (cis-PBO) (structure I) and poly(p-phenylene-trans-benzobisthiazole) (trans-PBT) (structure II).

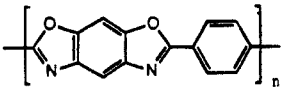

I

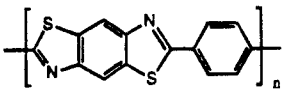

II

The accepted explanation for the high strength of PBZ fibers is that the molecules exist in solution in a rodlike conformation which leads to the formation of a nematic phase at sufficiently high concentration. The molecules in the anisotropic solution are readily aligned in the flow field during fiber spinning, resulting in a very high degree of molecular orientation parallel to the fiber axis.[1] The hypothesis regarding high backbone stiffness in solution is generally supported by both theoretical arguments[9] and solution studies.[1-8] Many questions remain, however, concerning the degree of backbone stiffness of the different members of the PBZ family as well as the connection between solution *vs* solid-state conformation. This is particularly the case with regard to cis-PBO, the subject of the present study.

Light scattering and viscometry are established techniques for studying chain dimensions and comparing the relative stiffness of various polymer chains. Problems that have been addressed range from helix-coil transition[10] to the effect of tacticity on chain dimensions of stereoregular polymers[11] and, more recently, to the stiffness of lyotropic liquid crystalline polymers.[12-16]

Berry and coauthors pioneered many studies on the molecular characteristics and physical behavior of PBZs[2,5-8] (in particular, trans-PBT), but some fundamental relationships, such as the intrinsic viscosity dependence on the molecular weight of cis-PBO, have not been firmly established. It is only recently that high molecular weight cis-PBO has become available.[4a] Earlier efforts to synthesize this molecule[4b] did not result in polymers of sufficient quality to permit systematic studies.

PBZs present unusual difficulties for molecular characterization. They do not dissolve in ordinary solvents; however, the polymers are soluble in strong anhydrous acids such as sulfuric acid (SA), chlorosulfonic acid (CSA), and methanesulfonic acid (MSA). Berry and his collaborators showed[2,8] that strong acids assist polymer dissolution by protonating the backbone and creating electrostatic repulsions between chains. These acids are difficult to characterize, and many nof their properties are not well quantified.[17] Their strongly corrosive and hygroscopic nature requires special equipment and handling precautions. In addition, small amounts of ionizable solutes, such as water and salts, have a profound influence on the solution behavior. The intrinsic viscosity $[\eta]$, in particular, is very sensitive to the ionic strength I of the solutions.

The dependence of $[\eta]$ on salt concentration in MSA saturated with methanesulfonic anhydride (MSAA) of two samples (samples 8 and 6 in Tables I and II) is shown in Figure 1. The $[\eta]$ initially drops sharply from the low ionic strength solvent (LIS) condition (no salt) with salt additions, followed by a shallow "plateau" region at higher ionic strengths[18] (HIS). Addition of water to the MSA-MSAA PBO solutions results in a similar behavior, but water content is difficult to quantify and control[17] accurately.

As will be shown, the concentration (C) dependence of the Rayleigh ratio[19] (R_θ) for cis-PBO in MSA is also affected by ionic strength. In the LIS regime the scattering behavior is complex, and the "Debye plots" appear highly curved, as illustrated in Figure 2 (higher curves). In the HIS regime, on the other hand, the scattering becomes well behaved, and the Debye plots become linearized, allowing for accurate extrapolations to infinite dilution, as shown also in Figure 2 (lowest data).

† Present address: Hewlett-Packard Laboratories, 3500 Deer Creek Rd., MS 26M, Palo Alto, CA 94303.

® Abstract published in *Advance ACS Abstracts*, August 15, 1993.

0024-9297/93/2226-5174$04.00/0

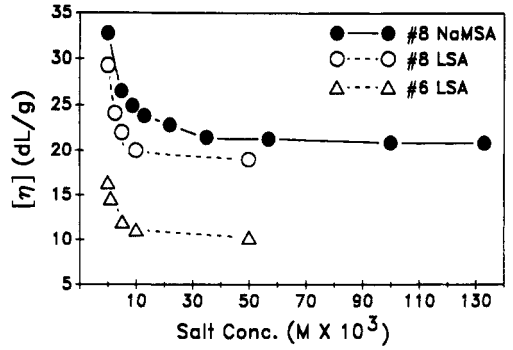

Figure 1. Effect of salt addition on intrinsic viscosity of *cis*-PBO initially dissolved in MSA saturated with MSAA: NaMSA addition to polymer sample 8 (filled circles), LSA addition to polymer sample 8 (open circles), and LSA addition to polymer sample 6 (open triangles).

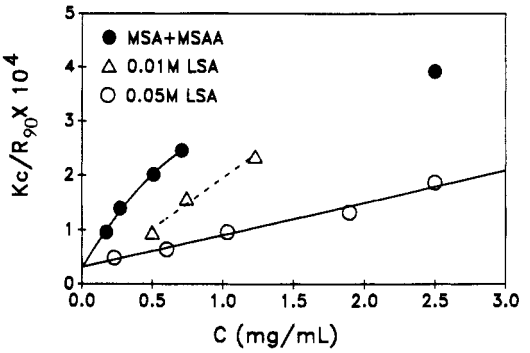

Figure 2. Reciprocal of the scattering intensity at 90°, (KC/R_{90}), *vs* polymer concentration (Debye plot) in the "vv" configuration for polymer sample 7 as a function of salt additions: no salt (filled circles), 0.01 M LSA (open triangles), and 0.05 M LSA (open circles). The data extrapolate to $M_{vv} \approx 32\,000$ at $C = 0$.

The HIS region, therefore, is an attractive solvent medium because the behavior of the PBO solutions appears to be reproducible, and the results become nearly independent of small ionic strength variations. This is in sharp contrast with the LIS regime in which slight ionic contaminations could lead to large uncertainties.

The salt concentration dependence of $[\eta]$ is not well understood. If *semistiff* chain behavior is assumed, on the one hand, Figure 1 may be explained in terms of the screening of electrostatic contributions to chain stiffness. If the chains are *ideal rods*, on the other hand, intramolecular screening would not affect chain conformation. Berry and co-workers have suggested[7,8] that this behavior may be caused by the formation of parallel dimers, trimers, etc. (aggregation) as intermolecular repulsions become screened out by counterions. In the present study, the relationship between $[\eta]$ and the *apparent* M_w and the dependence of R_g on the *apparent* degree of polymerization are analyzed in terms of the semistiff chain hypothesis. The results are compared to statistical persistence lengths estimated with simple virtual bond approximations of the actual chain. The model is based on the geometry of the repeat unit obtained by *ab initio* molecular orbital calculations.

Theoretical Background

The apparent molecular characteristics of PBO in MSA–MSAA (HIS) solutions were determined from the total scattering intensity of dilute solutions as functions of concentration C and scattering angle θ. Stiff linear molecules are optically anisotropic and their light scattering results require depolarization corrections.[5,6,12,13] The optical anisotropy, δ, was determined from the ratio between the vertical and horizontal components, R_{vv} and R_{hv}, of the Rayleigh ratio using vertically polarized incident light:

$$\frac{1}{M_{vv}} = \left(\frac{KC}{R_{vv}}\right)_0 = \lim_{\substack{\theta\to 0\\ C\to 0}} \frac{KC}{R_{vv}} \tag{1}$$

$$\frac{1}{M_{hv}} = \left(\frac{KC}{R_{hv}}\right)_0 = \lim_{\substack{\theta\to 0\\ C\to 0}} \frac{KC}{R_{vh}} \tag{2}$$

$$\frac{M_{hv}}{M_{vv}} = \frac{3\delta^3}{5 + 4\delta^2} \tag{3}$$

where M_{vv} and M_{hv} are apparent molecular weights from the vv and hv measurements, $K = 4\pi^2(\partial n/\partial C)^2 n^2/(N_A \lambda_0^4)$ is the optical constant,[19] $n = 1.424$ is the solvent refractive index,[17] $\partial n/\partial C = 0.48 \pm 0.01$ mL/g is the refractive index increment of PBO in MSA, $\lambda_0 = 633$ nm is the wavelength of the He–Ne laser, and N_A is Avogadro's number.

For stiff backbone polymers, the anisotropy correction on the weight-average molecular weight, M_w, may be approximated with[6,12,13]

$$M_w = \frac{M_{vv}}{1 + (4/5)\delta^2} \tag{4}$$

The radius of gyration, R_g, can be estimated from

$$\lim_{C\to 0}\left(\frac{KC}{R_{vv}}\right) = \frac{1}{M_{vv}}\left(1 + \frac{R_{g,vv}{}^2 q^2}{3} + \ldots\right) \tag{5}$$

$$R_g{}^2 = \frac{1 + (4/5)\delta^2}{1 - (4/5)\delta + (4/7)\delta^2} R_{g,vv} \tag{6}$$

where $q = (4\pi n/\lambda_0)\sin(\theta/2)$ is magnitude of the scattering vector. Finally, the second virial coefficient can be determined from

$$A_2 = A_{vv}(1 + (4/5)\delta^2)^2 \tag{7}$$

where A_{vv} is the apparent second virial coefficient in the "vv" configuration:

$$\lim_{\theta\to 0} \frac{KC}{R_{vv}(\theta)} = \frac{1}{M_{vv}}[1 + 2A_{2,vv}M_{vv} + \ldots] \tag{8}$$

As the molecular weight increases, the anisotropy corrections become smaller, *i.e.*, $\delta \to 0$, and $M_{vv} \to M_w$, $R_{g,vv} \to R_g$, and $A_{2,vv} \to A_2$.

Assuming semistiff chain behavior, the results may be described in terms of an effective persistence length,[15,16] Q:

$$R_g{}^2 = Q^2\left(\frac{y}{3} - 1 + \frac{2}{y} - \frac{2}{y^2}[1 - e^{-y}]\right) \tag{9}$$

$$\delta^2 = \delta_0{}^2\left(\frac{2}{3y} - \frac{2}{(3y)^2}[1 - e^{-3y}]\right) \tag{10}$$

where $y = L/Q$ and L is the contour length of the chain. The relationship between intrinsic viscosity and molecular weight can be expressed in terms of wormlike chain polynomial expressions F derived by Yamakawa and Fujii[20] (YF):

$$[\eta] = F_i(y, d, M_L) \tag{11}$$

where d is the chain diameter and M_L is the "shift factor", equal to the "effective" molecular weight per unit length of chain (Appendix A). These dimensions may be obtained from crystallographic data.[21] For semistiff chains, eq 11 does not follow a single power dependence on M_w, and the so-called Mark–Houwink relationship was "generalized",

MH(G), to include nonlinear terms in the log–log form of the relationship.

Experimental Methods

Sample preparations and measurements were performed in an environmentally controlled laboratory with relative ambient humidity lower than 10% at all times. Additional precautions were taken to minimize water uptake, such as storing the glassware at ~115 °C in a convection oven and storing samples under a continuous flow of dry N_2.

Commercial MSA (Fluka Chemika and Aldrich Chemical Co.) was distilled[17] through a 40-cm Vigreux column under vacuum (~1 mmHg) at 160 °C in the presence (~6 wt %) of phosphorus pentoxide (P_2O_5). The initial distillation fractions consisted of the MSAA-rich low melting point (~70 °C) solid, and the latter fractions consisted of MSA with variable amounts of MSAA and H_2O. The solvents were standardized by saturating the MSA fractions with MSAA at 25 °C to control the water content of the solutions. The salts CH_3SO_3Na (NaMSA), LiF_3CSO_3 (LTF), and Li_2SO_4 (LSA) were purchased from Aldrich Chemical Co. and were used as received. Possible water contamination of the MSA–MSAA salted solvents was checked by proton NMR and viscometrically as discussed in ref 17.

Kinematic viscosities were measured using Ubbelohde capillary viscometers in a thermostatic bath (Schott Gerate Model CT 1450) at 25 ± 0.02 °C. The viscometer running times were usually in the range 100–500 s. Kinetic energy (Hagenbach) corrections were negligible (<0.04 s for flow times ≥80 s). Shear stress dependence was checked with a four-bulb viscometer using sample 7 ([η] = 15.7 dL/g); the sample did not show significant dependence. Amis and co-workers[18] have confirmed this result using a low shear rate viscometer.

Refractive index increments were measured in a G. N. Woods differential refractometer (Newton, PA), and optical absorbances were measured with a Shimadzu Model UV-160 spectrophotometer.

Light scattering measurements were carried out with an Otsuka Model DLS-700 apparatus (sold by Polymer Laboratories). The instrument was initially equipped with a 5-mW He-Ne laser, which was later replaced with a 15-mW unit to improve depolarized scattering resolution. A narrow-band rejection filter was installed in front of the photomultiplier tube, and two Glan-Thompson prisms mounted on a rotating stage were used for "hv" and "vv" scattering. During operation, the scattering cell (21-mm diameter) was surrounded by a thermostatic and "refractive index matching" bath of di-*n*-butyl phthalate (n_d = 1.490) at 25 °C. The instrument calibration and alignment were routinely verified with a secondary standard, spectrophotometer grade toluene (J. T. Baker, Inc.). A polystyrene standard ($M_w = 3.55 \times 10^5$, $M_w/M_n = 1.02$) was used initially to verify the DLS-700 performance.

The scattering cells were washed in an ultrasonic bath using MICRO glass cleaning solution (International Products Corp., Trenton, NJ) and thoroughly rinsed with high-purity filtered water.

In the early part of this work, the solvents were filtered repeatedly through 0.2-μm PTFE filters with the purpose of sweeping away hypothetical downstream particulates. It was later found that a new type of inorganic filter (ANOTOP, pore size 0.02 μm) yielded considerably lower levels of particulates. These filters were used for very short times (2–3 min was required to filter 3–5 mL of HIS MSA–MSAA) and only for *HIS solvents* (0.1 M NaMSA and 0.05 M LSA). The scattering behavior of PBO in *HIS conditions* showed no dependence on filtering device. The inorganic filters were not used for solvents at low salt concentrations, however, such as those shown in Figure 2.

cis-PBO stock solutions were usually filtered through polypropylene-encapsulated 0.45-μm PTFE filters (Micron Separations) and then added stepwise to the scattering cells containing filtered solvents. Each new concentration was gently mixed in the scattering cell and then spun for 3–8 h in a centrifuge (Sorval Model RC-2B) at ~2800*g* (4000 rpm).

Thirteen PBO samples representing a broad range of intrinsic viscosities (from [η] = 1.4 dL/g to [η] = 50 dL/g) were studied. The samples were synthesized in the nematic phase (14% PBO concentration in PPA) as described by Wolfe.[4b] The lower [η] samples (samples 1–5) were synthesized using ordinary 1-L kettle reactors. The syntheses of the first four samples were stoichiometrically designed to achieve predetermined degrees of polymerizations. Samples 6–13, on the other hand, were synthesized using a more powerful mixing device (piston reactor) as discussed by Ledbetter and coauthors,[4a] and the reaction mixtures were sampled at various stages in the polymerizations.

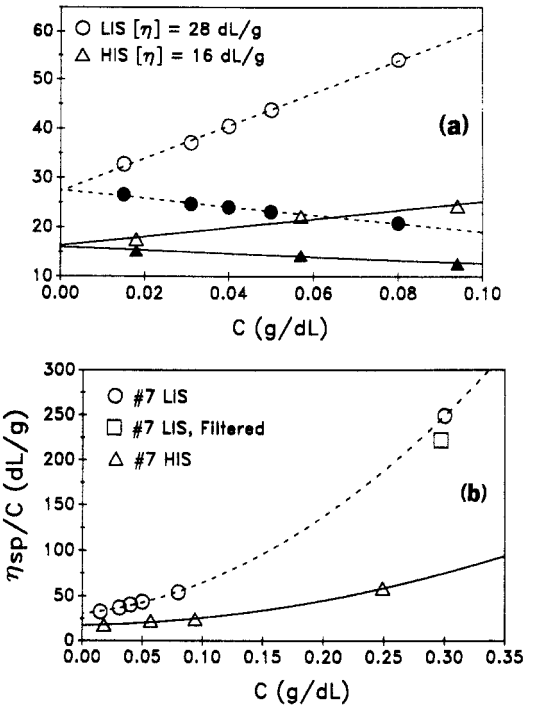

Figure 3. (a) Intrinsic viscosity double extrapolation of sample 7 in low ionic strength (LIS) solvent (circles) and in 0.05 M LSA high ionic strength (HIS) solvent (triangles). The Huggins and Kraemer coefficients are $k' = 0.45$ and $k'' = 0.11$ for the LIS data and $k' = 0.35$ and $k'' = 0.133$ for the HIS data. Note that $k' - k'' \approx 0.5$. (b) Higher concentration behavior of η_{sp}/C for sample 7 in LIS (open circles) and HIS (open triangles) solvents. The LIS solution appears to deviate more strongly from the linear behavior than the HIS solutions. The square datum corresponds to a filtered solution (0.45-μm filter). The high viscosity of this sample is a good indication that this sample did not become contaminated with ions or ionizable bases (such as water) during filtration and that the filter did not fractionate the polymer.

Results

(A) Intrinsic Viscosity. The intrinsic viscosities [η] of representative PBO samples were determined from the Huggins and Kraemer relations[22]

$$\frac{\eta_{sp}}{C} = [\eta] + k'[\eta]^2 C + \ldots \quad (12)$$

$$\frac{\ln(\eta_{rel})}{C} = [\eta] + k''[\eta]^2 C + \ldots \quad (13)$$

by extrapolation to zero concentration. In eqs 12 and 13 $\eta_{rel} = \eta_{soln}/\eta_{solv}$ and $\eta_{sp} = \eta_{rel} - 1$.

The kinematic viscosity of the LIS solvent (MSA saturated with MSAA) was $\eta_{solv} = 9.8 \times 10^{-6}$ to 9.9×10^{-6} $m^2\ s^{-1}$ (centistokes) at 25 °C. The viscosities of the HIS solvents, on the other hand, were functions of salt concentration and salt type. For MSA–MSAA with 0.1 M NaMSA, the kinematic viscosity is $\eta_{solv} = 11 \times 10^{-6}$ $m^2\ s^{-1}$.

The plots corresponding to eqs 12 and 13 (Figure 3a) were reasonably linear for solutions in MSA–MSAA solvent *without* salts (LIS) and in HIS conditions in the range 0.02–0.1 g/dL with $k' \sim 0.5 \pm 0.15$ (sample 7). The higher viscosity of the solution in LIS solvent relative to the HIS solvent is quite apparent. The viscosity behavior of solutions in LIS solvents, however, was very sensitive to

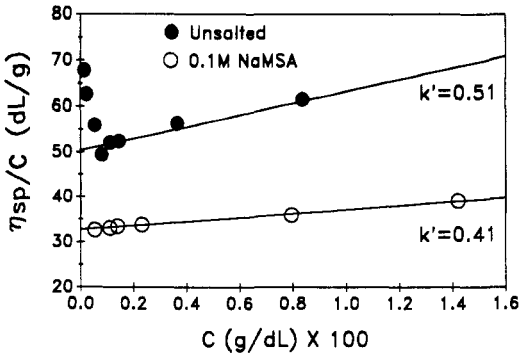

Figure 4. Low concentration limiting behavior of η_{sp}/C in LIS and HIS solvents of a sample similar to sample 11. The intrinsic viscosities are $[\eta] = 50$ and 33 dL/g, respectively. The HIS sample (open circles) is well behaved throughout the concentration range, but the LIS sample shows anomalous behavior at very low polymer concentrations. This behavior was not very reproducible, however, due to the extreme sensitivity of the solution viscosity to traces of water and other contaminants.

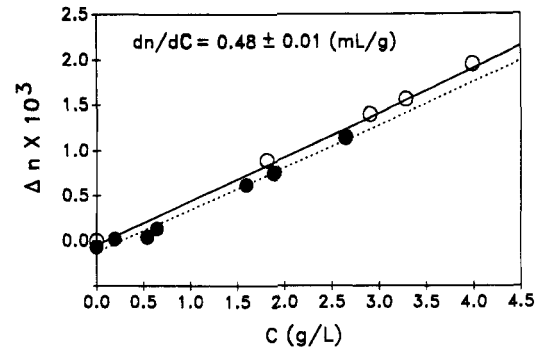

Figure 5. Differential refractometry of *cis*-PBO in MSA–MSAA with 0.1 M NaMSA for two independent solutions. The slope of the data corresponds to $dn/dC = 0.48$ mL/g, and it is in very good agreement with the reported value in MSA.

slight water contamination. To obtain linear plots such as the one in Figure 3a, extremely dry experimental conditions throughout the series dilutions were usually required. The behavior of samples in HIS solvent conditions, on the other hand, was usually linear and very reproducible (within ~5%).

Figure 3b shows the viscosity behavior of sample 7 at higher concentrations. Deviation from linearity becomes apparent in the neighborhood of $C[\eta] > 3$, and it is more pronounced in LIS solvent than in HIS solvent. The specific viscosity of a LIS solution after filtration (0.45-μm PTFE filter) is also shown (square datum). The viscosity difference between the filtered and unfiltered samples is small, suggesting that filtration does not cause major fractionation or polymer degradation. This also suggests that the sample (in LIS solvent) did not become seriously contaminated with water or other ionizable compounds during filtration; such contamination would have resulted in a dramatic drop in viscosity, as discussed above.

Figure 4 shows the extreme dilution limit ($C < 0.01$ g/dL) of sample 11 ($[\eta] = 32$–33 dL/g) without salts (circles, $k' = 0.51$) and with salts (squares, $k' = 0.4$). In this figure, the salted solution shows "normal" extrapolation behavior. The salt-free solution, on the other hand, shows anomalous behavior at very low concentrations (rapid viscosity upswing). This behavior, however, was observed near the resolution limit of the viscometer ($\eta_{rel} < 1.02$), and it was difficult to reproduce.

Since the purification and conditioning process of MSA is difficult and time-consuming, $[\eta]$ was estimated from a "single-point" approximation to the $\lim_{C\to 0}(\eta_{sp}/C)$ extrapolation. An approximate formula was derived by expanding the natural logarithm in the power series

$$\ln(\eta_{rel}) = \eta_{sp} - (1/2)\eta_{sp}^2 ... \qquad (14)$$

and by substituting this relationship into linear combinations of eqs 12 and 13

$$\frac{\eta_{sp} + 3\ln\eta_{rel}}{4C} = [\eta] + (k' - 3/8)[\eta]^2 C + ... \qquad (15)$$

The real positive root of this equation is given by

$$[\eta] \approx \frac{-1 \pm [1 + (z - 3/8)(\eta_{sp} + 3\ln\eta_{rel})]^{1/2}}{2(z - 3/8)C} \qquad (16)$$

where $z \approx k'$ could be used as an adjustable parameter. It was determined that $z = 0.5$ resulted in excellent agreement with the extrapolated $[\eta]$ values when η_{rel} was measured between $C = 0.02$ and 0.05 g/dL. The $[\eta]$'s of the PBO samples in MSA–MSAA in the HIS regime are listed in the second column of Table I. Repeated measurements of several samples with different salts indicated $[\eta]$ reproducibility better than ~10%.

(B) Light Scattering. Toluene was used as a secondary intensity standard. The Rayleigh ratio for vertically polarized incident and scattered light was given by

$$R_{vv}(\theta) = \left(\frac{n_s}{n_t}\right)^2 [\Delta I/I_t] R_{vv,t}(90°) \sin(\theta) \qquad (17)$$

where $n_s = 1.424$ and $n_t = 1.49$ are the refractive indices of the solvent and of toluene, respectively, ΔI is the scattering of the PBO solutions (corrected for absorbance) minus the solvent, I_t is the scattered intensity of toluene, and the Rayleigh ratio $R_{vv,t}(90°) = 10.566 \times 10^{-6}$ cm^{-1} was assumed for toluene.[23] An equivalent relationship to eq 18 was used for R_{hv} with $R_{hv,t}(90°) = 3.434 \times 10^{-6}$ cm^{-1}.

The value $dn/dC = 0.48 \pm 0.01$ mL/g was obtained for PBO in MSA–MSAA (Figure 5). This result is very close to the reported[6] $dn/dC = 0.474$ mL/g in MSA without MSAA. The salts apparently do not affect dn/dC significantly. Although dn/dC is nearly independent of MSA–MSAA composition, the refractive index of the solvent itself shows variability with MSAA composition.[17] For this reason, dn/dC measurements demanded very accurate solvent composition matching.

PBO solutions in MSA were generally bright yellow and showed low absorbances at $\lambda = 633$ nm. The lower $[\eta]$ samples (kettle reactions 1–5), however, showed slight bluish discolorations and higher absorbances than the high-$[\eta]$ samples (Figure 6). The discoloration was attributed to oxidized chain end groups (diaminoresorcinol, the PBO monomer, becomes strongly bluish in solution in the presence of air). The high-$[\eta]$ samples (piston reactor) showed specific absorbances in the neighborhood of $\epsilon \approx 0.025$ L g^{-1} cm) at $\lambda = 633$ nm. It appears that the more efficient agitation and oxygen-free polymerization conditions of the piston reactor quenched the formation of the chromophores.

The scattering intensity of the MSA–MSAA solvent was considerably lower than that of toluene ($R_{vv,solv}(90°) \approx 1.43 \times 10^{-6}$ cm^{-1}). The depolarized scattering $R_{hv,solv}(90°)$ of MSA–MSA was very low (2.75×10^{-7} cm^{-1}, $\rho_v \approx 0.19$); this is near the background noise level of the instrument. The angular independences of $R_{vv,solv}$ (within 2%) and toluene (within 1%) in the range 30–150° were used to check for dust.

PBO solution scattering was usually investigated with four to six concentrations in the range from $C = 0.02$ g/L

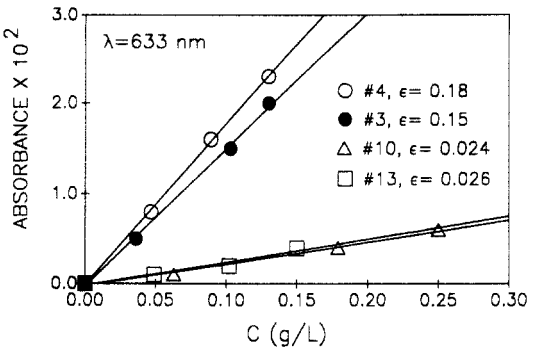

Figure 6. Optical absorbances of several *cis*-PBO samples in MSA–MSAA with 0.1 M NaMSA. The more strongly absorbing samples are the low molecular weight samples 3 (filled circles) and 4 (open circles) in Tables I and II. Samples 10 (open triangles) and 13 (open squares) were typical of high molecular weight samples. The stronger absorbances of the low molecular weight samples were attributed to chain ends.

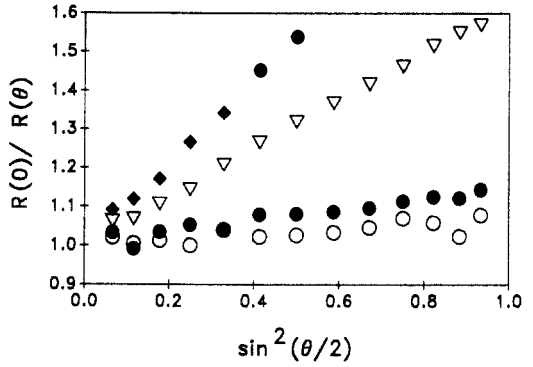

Figure 7. Angular dependence of the reciprocal of the scattering intensity ($\Delta R(0)/\Delta R(\theta)$ in the "vv" optical configuration of low-M_w samples (sample 1, open circles, and sample 4, filled circles) and high-M_w samples (sample 8, open triangles, and sample 11, filled diamonds) in MSA–MSAA with 0.1 M NaMSA. The scattering angular dependence appears to be reasonably linear for all samples. The absence of strong downward curvature at the lower angles suggests that there are no large aggregates (*ca.* 1 μm) and that the samples are relatively free of dust.

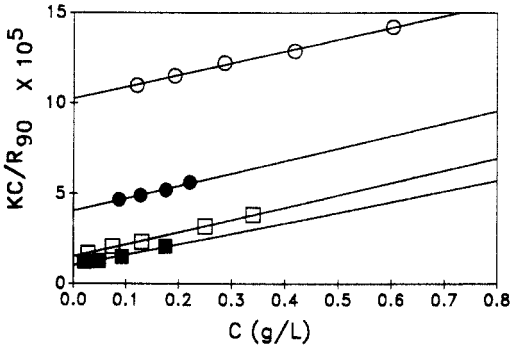

Figure 8. Debye plots ("vv" configuration) in MSA with 0.1 M NaMSA of several samples at 90°. Sample 1 (open circles), A_{vv} = 0.036; sample 4 (filled circles), A_{vv} = 0.034; sample 9 (open squares), A_{vv} = 0.034; sample 13 (filled squares), A_{vv} = 0.029 A_{vv} in cm^3 g^{-2} mol).

to C = 0.25 g/L and between 30° and 150° (10° intervals). The data obtained at the lowest angle, 30°, were occasionally disregarded because of dust interference, but generally the plots between 30° and 150° did not show much curvature (Figure 7). The absence of strong downward deviations at the lower angles suggests the absence of "large" aggregates (~1 μm) in these solutions.

Typical plots of $KC/R_{vv}(\theta)$ against C (Debye plots) are shown in Figure 8 for low and high M_w's. The scattering intensities of the samples were usually well above the solvent scattering. For example, the scattering of the

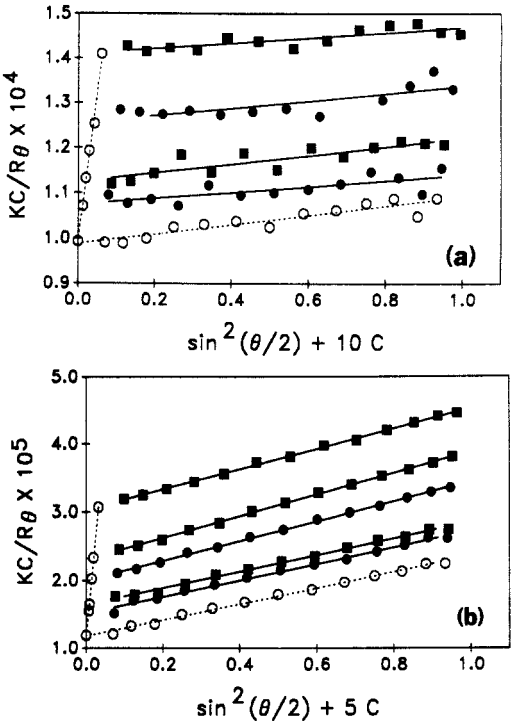

Figure 9. (a) First-order (linear) Zimm plot ("vv" configuration) of the lowest M_w sample (sample 1) in MSA–MSAA with 0.1 M NaMSA. The concentrations are 0.12, 0.192, 0.419, and 0.96 g/L. They correspond to the alternating rows of filled squares and circles (from bottom to top, respectively). The open circles correspond to the extrapolations to C = 0 (botton row) and θ = 0 (left line). The extrapolated molecular weight is M_{vv} = 10.4 K. (b) Zimm plot ("vv" configuration) at a high-M_w sample (sample 8) in MSA–MSAA with 0.1 M NaMSA. The concentrations are 0.031, 0.043, 0.071, 0.093, and 0.16 g/L. The plot extrapolates to M_{vv} = 84K.

lowest concentration (C = 0.02 g/L) of sample 8 ([η] ≈ 20 dL/g) was nearly 2 times stronger than the solvent in the "vv" configuration and 3 times stronger than the solvent in the "hv" configuration.

The initial studies showed that while increasing salt concentration strongly affected the C dependence of the intensity (A_2), it did not appear to affect the $C \rightarrow 0$ extrapolation, as illustrated in Figure 2. This is an important observation, since it suggests that aggregation is not increasing with salt concentration for dilute PBO solutions. The accuracy of the $C \rightarrow 0$ extrapolations, however, increased dramatically as the data became linearized with increasing salt concentration.

The Zimm plots of PBO in HIS solutions showed relatively normal scattering patterns for low as well as high molecular weights (Figure 9).

The salt LSA was used during the earlier part of the studies, but NaMSA was later used. Solution viscosity experiments using both salts[17,18] showed very similar behavior between NaMSA and LSA at comparable ionic strengths. The scattering behavior of sample 1 was studied using LSA as well as NaMSA. Within experimental error, the M_w estimates were identical for both salts ($M_w \approx$ 7000–8000). LTF was also used for samples 9 and 11, but conductivity experiments later suggested that this salt may not be completely dissociated in MSA.

The scattering intensity in the "hv" configuration was not clearly resolved by the instrument initially equipped with a 5-mW He–Ne laser. The extrapolations indicated by eq 2 resulted in only $M_{hv} \approx$ 1000 for most samples. After replacement by a more powerful light source (15 mW), the instrument was able to resolve the "hv" scattering

Table I. Intrinsic Viscosity and Light Scattering Results

PBO	[η] (dL/g)	salts in [η]	$M_w \times 10^{-3}$	salts in LS	$M_{vv} \times 10^{-3}$	$M_{hv} \times 10^{-3}$	δ	$(R_g^2)^{1/2}$ (nm)	A_2 ($cm^3\ g^{-1}$ mol)
1			7.5	0.05 M LSA	9.5				
	1.4	0.1 M NaMSA	8.1	0.1 M NaMSA	10.2	1.6	0.57	25	0.06
2	2.72	0.1 M NaMSA	15[a]	0.05 M LSA	18	2.3[a]	0.51[a]	33	0.051
			15.6[b]			1.8[b]	0.44[b]		
3	2.9	0.1 M NaMSA	14.6	0.1 M NaMSA	18	2.5	0.54	19	0.046
			15.6[b]			1.8[b]	0.44[b]		
4	4.4	0.1 M NaMSA	23	0.1 M NaMSA	26.2	1.9	0.37	29	0.057
5	5.0	0.05 M LSA	19[a]	0.05 M LSA	21	2.3[a]	0.46	28	0.045
	5.4	0.1 M NaMSA							
6	10.3	0.05 M LSA	38[a]	0.05 M LSA	40	2.3[a]	0.32	43	0.038
7	15.7	0.1 M LSA	45[a]	0.05 M LSA	47	2.3[a]	0.3	48	0.034
	15.6	0.05 M LSA							
8	20.3	0.1 M NaMSA	82	0.1 M LTF	84	2.6	0.24	64	0.043
9	20.8	0.1 M NaMSA	92[a]	0.1 M LSA	95	2.3[a]	0.2	66	0.03
10	24.9	0.1 M NaMSA	112	0.1 M NaMSA	116	2.8	0.2	78	0.038
11	28.3	0.1 M NaMSA	116	0.1 M LTF	120	2.3	0.18	85	0.03
12	37	0.05 M LSA	~200[a,c]	0.05 M LSA	220	2.3[a]	0.13	96	0.03
13	50	0.1 M NaMSA	~250[c]	0.1 M NaMSA	230–290	2.5	0.125	113	0.03

[a] The value $M_{hv} \approx 2300$ was assigned to this sample. The low-power laser (5 mW) was used to measure this sample. [b] The value $M_{hv} \approx 1800$ resulted in better agreement with Flory's polydispersity index, and $\delta = 0.44$ shows better agreement with the anisotropy data trend in Figure 14. [c] This sample showed considerable M_w extrapolation uncertainty.

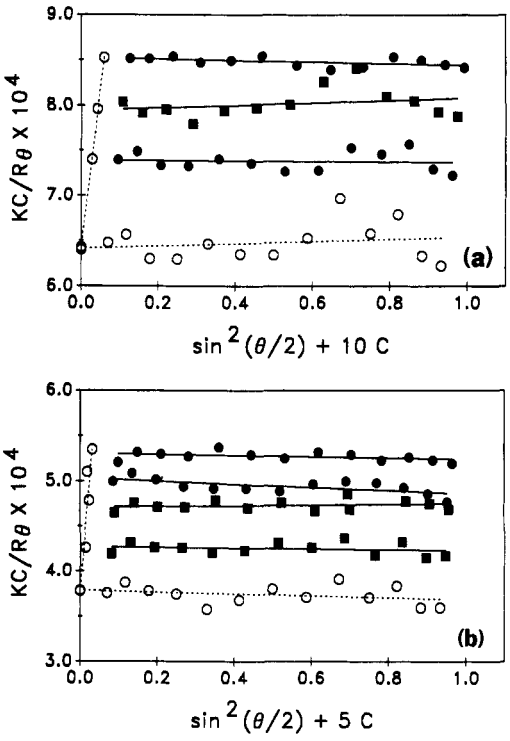

Figure 10. (a) Zimm plot of sample 1 in MSA–MSAA with 0.1 M NaMSA in the "hv" optical configuration. The concentrations are 0.286, 0.419, and 0.603 g/L. There is considerable uncertainty in the data due to the low scattering intensity. The plot extrapolates to M_{hv} = 1.6K. (b) Zimm plot of sample 8 in the "hv" optical configuration. The concentrations are 0.071, 0.093, 0.117, and 0.16 g/L. The plot extrapolates to M_{vh} = 2.67K.

(Figure 10), with M_{hv} = 1600 for sample 1 and $M_{hv} \approx 2300$ for the higher molecular samples. This value is in good agreement with reported results,[5,6] but the Zimm plot extrapolations of the depolarized scattering showed considerable uncertainty for some samples (±500).

The samples that had been initially measured with the 5-mW laser were *assigned* the value M_{hv} = 2300, as indicated in Table I. This assignment introduces some uncertainty in the molecular parameters for the low molecular weight samples 2, 5, and 6. The depolarization corrections, however, become smaller than the experimental errors (~10%) for the higher molecular weight samples (samples 7, 9, and 12).

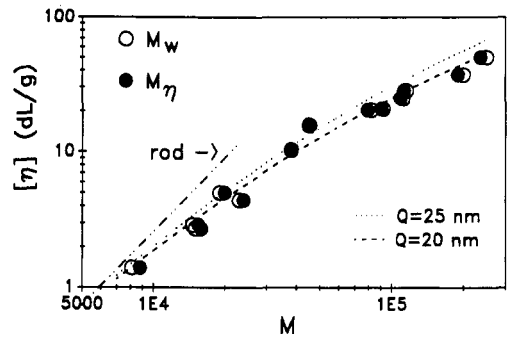

Figure 11. Correlation between intrinsic viscosity [η] and M for *cis*-PBO in salted MSA–MSAA solutions. The open circles correspond to the measured M_w, and the filled circles to the *estimated* M_η. The theoretical curves of the Yamakawa–Fujii wormlike chain model are also shown. The dotted line corresponds to the persistence length Q = 25 nm, and the dashed line to Q = 20 nm. Nearly identical curves were calculated assuming d = 0.5 and 0.6 nm and M_L = 200 and 203 (Da/nm), respectively. The rigid rod limit behavior is also shown for comparison.

Table II. Polydispersity Ratio of Well-Defined Samples

sample	[η] (dL/g)	N_w	N_n	method for N_n	N_w/N_m
1	1.4	34.6	21	stoichiometry	1.65
2	2.7	64	42.7	stoichiometry	1.5
		66.7[a]			1.56[a]
3	2.9	62.4	35.6	end labeled	1.75
		66.7[a]			1.87[a]
4	4.4	101.4	52	end labeled	1.95

[a] This value is obtained by correcting for anisotropy with $\delta \approx 0.44$.

Analysis

(A) Correlation between M_w and [η]. Tables I and II summarize the light scattering and viscometric studies in high ionic strength solutions. The MH(G) relationship is shown in Figure 11 (filled circles). In this figure, the ideal "rigid-rod" relationship[24]

$$[\eta]_{rr} = \frac{\pi N_A L^3}{24M[\ln(L/d) + 2\ln(2) - 7/3]} \tag{18}$$

is also shown for comparison.

The data were approximately fitted with the YF wormlike model (eq 11) for several values of the persistence length Q assuming shift factors $M_L = M_0/L_0$ = 196–203 Da nm^{-1} and chain diameters d = 0.5–0.6 nm (Appendix A).

The approximate shift factors were estimated by assuming that each PBO repeat unit (M_0 = 234 g) contributes L_0 = 1.15–1.19 nm along the chain axis. These lengths differ from the crystallographic value,[21] L_0 = 1.205 nm, because it was assumed that the *diprotonated* repeat unit is slightly more bent than the unprotonated case (see Discussion). The effective chain diameter d = 0.5 nm was estimated from the cross-sectional area of the chain in the crystal[21] (0.194 nm^2). In the diprotonated state, the effective diameter is probably slightly larger, assuming that the relaxation of the ionic cloud around the chain is much faster than the rotational relaxation of the polymer.

The third-order least-squares regression through the log–log data is given by

$$Y = -9.226 + 3.0121X - 0.09274X^2 - 0.017X^3 \quad (19a)$$

and its inverse is given by

$$X = 3.8041 + 0.8845Y - 0.3312Y^2 + 0.2244Y^3 \quad (19b)$$

where $y = \log([\eta])$ and $X = \log(M_w)$. These curves are very close to the YF model prediction with Q = 20 nm ($d \approx 0.5$ nm and M_L = 200 Da nm^{-1}) as shown in Figure 11. Assuming the crystallographic length L_0 = 1.205 nm (M_L = 194) and d = 0.5 nm, the model also shows good data fitting, but with lower persistence length ($Q \approx 18$ nm).

An error analysis of the results suggested that the data are distributed homogeneously around the regression curve (eq 19a) regardless of the salt used for each individual measurement. The region of 90% acceptance error is 1.36σ, which results in an estimated overall uncertainty of $\pm 0.2M_w$.

(B) Polydispersity. The polydispersity ratios[25] PDR = M_w/M_n, where N's are the corresponding average degrees of polymerization, were estimated for samples 1–4. These samples were stoichiometrically designed to achieve definite M_n's and were endcapped with a monoacid. Samples 1 and 2 were designed for M_n = 5000 (N_n = 21.4) and M_n = 10 000 (N_n = 42.7), respectively. Samples 3 and 4 were endcapped with F-derivatized groups, and their degrees of polymerization were assessed spectroscopically.[26] Table II compares the estimated N_n's with the measured N_w. The PDRs are smaller (PDR ~ 1.5–1.95) than the value expected from Flory's most probable distribution (PDR = 2). The PDRs, however, are probably closer to the upper value since the N_n's of samples 3 and 4 (PDR = 1.75–1.95) were better characterized. In addition, the M_{hv} entries for samples 2 (2300) and 3 (2500) are conservatively large. Reducing these values to $M_{vh} \approx 1800$ (an intermediate value between those of samples 1 and 4) would lead to $\delta \approx 0.44$ and $M_w \approx 15\,600$ for samples 2 and 3, resulting in PDR = 1.87–1.95 for samples 3 and 4.

Polydispersity affects the MH(G) relationship since viscosity measures the "viscosity-average" molecular weight,[25,27] M_η. This average is a function of the Mark–Houwink exponent α of the polymer and can be approximated by

$$M_\eta/M_w = \frac{[(1+\alpha)\,\Gamma(1+\alpha)]^{1/\alpha}}{2} \quad (20)$$

where $\Gamma(1+x)$ is the gamma function. Since in this case the exponent changes as a function of M_w, the α exponent may be estimated by differentiating eq 19a or eq 11 with Q = 20 nm.

$$\alpha \approx \frac{\partial \log([\eta])}{\partial \log(M_w)} \quad (21)$$

The approximate values of α *vs* M_w are shown in Figure 12. The wormlike chain model estimates a narrower range

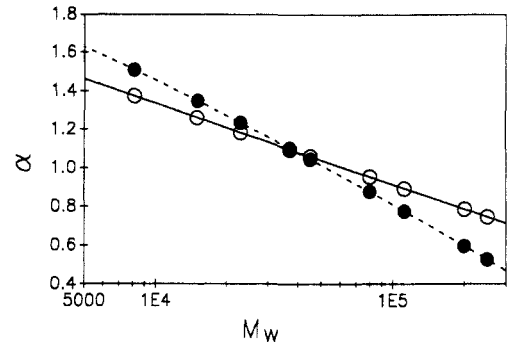

Figure 12. Mark–Houwink exponents, α, as a function of molecular weight (semilogarithmic plot) estimated from the wormlike chain model with Q = 20 nm, eq 11 (closed circles), and from the data least-squares fit, eq 19a (open circles). The exponent changes from $\alpha \approx 1.4$–1.5 at M_w = 8K to $\alpha \approx 0.6$–0.8 at M_w = 200K. The agreement between the two curves is reasonably good, but the data show steeper change of α with M_w than the model.

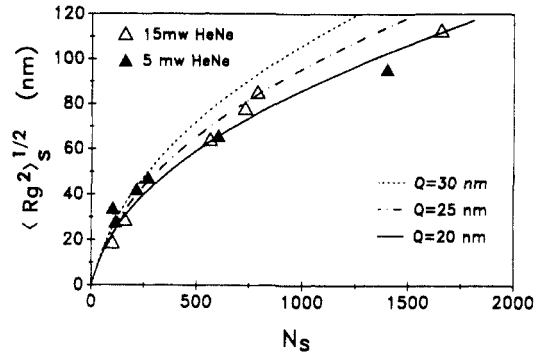

Figure 13. Correlation between measured radius of gyration, R_g, and estimated degree of polymerization, N_s (M_s/234). Open triangles correspond to data obtained with the 15-mW He–Ne laser light source, and the closed triangles correspond to data obtained with the 5-mW laser. The curves correspond to the wormlike chain model (eq 9) for several values of the persistence length Q.

of α's because the curvature of eq 19a is somewhat accentuated by the high molecular weight samples 12 and 13 (~200K). More data points would be desirable in this range since sample 13 showed considerable M_w uncertainty.

The intrinsic viscosity data plotted against M_η are the open circles in Figure 11. The differences between M_w and M_η are small because $\alpha \approx 1.4$–0.9 (from low to high M_w).

(C) Chain Dimensions. The relationship between R_g and the degree of polymerization also deviates from ideal rodlike behavior. For polydisperse semistiff chains, the experimental R_g corresponds to a so-called "s" average. The corresponding molecular weight average is given by[28]

$$M_s = (M_w^{-1}\sum_i w_i M_i^{1+p})^{1/p} \quad (22)$$

where p = 1 for Gaussian coils ($M_s = M_z$) and p = 2 for rods. These limits correspond to $M_s = (3/2)M_w$ for coils and $M_s = 3^{1/2}M_w$ for rods[29] assuming Flory's most probable distribution. Appendix B shows a method to approximate $M_s(p)$ for wormlike chains in the neighborhood of Q = 20 nm.

Figure 13 shows R_g *vs* the most probable distribution s-average degree of polymerization, N_s, and the curves for the wormlike chain model (eq 9) with several values of Q. The agreement between the data and the wormlike chain model in the neighborhood of Q = 20–25 nm is very good.

The relationship between the optical anisotropy δ and N_w is shown in Figure 14. In principle, this relationship

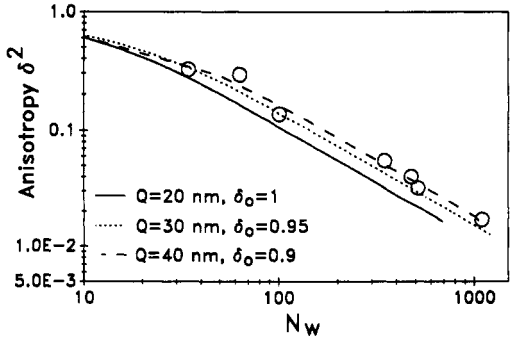

Figure 14. log–log plot of the square of the optical anisotropy, δ^2, *vs* the weight-average degree of polymerization, N_w. The open circles correspond to data obtained with the 15-mw He–Ne laser as indicated in Table I. The curves correspond to the wormlike chain model (eq 10) for several values of Q and the specific anisotropy δ_0.

can be used to estimate backbone stiffness[16] using eq 10. This approach, however, is very sensitive to the choice of δ_0, a quantity which is difficult to determine since it requires long extrapolations or light scattering studies of very low M_w samples. For the well-studied case of poly(1,4-phenyleneterephthalamide) (PPTA), for instance, values ranging from $\delta_0 \approx 0.5$ to 0.75 have been reported,[6,16] corresponding to stiffness between $Q \approx 15$ nm and 45 nm.

Assuming δ_0 = 0.95–0.90 for *cis*-PBO, the anisotropy behavior is in reasonable agreement with the wormlike chain model with $Q \sim 30$–40 nm. The anisotropy appears to be considerably higher for *cis*-PBO than for *trans*-PBT[8] ($\delta_0 \approx 0.53$–0.75). This is in qualitative agreement with the computational estimates of Bhaumik and co-workers.[30]

The datum corresponding to sample 3 ($\delta_0 \approx 0.54$, second point from the left) in Figure 14 deviates considerably from the trend. The value $\delta_0 \approx 0.44$ suggested earlier in the text is probably more appropriate.

(D) Second Virial Coefficient. The second virial coefficient A_2 of the solutions decreased with ionic strength as shown in Figure 2. The change was rather dramatic for nearly salt-free samples, but it became less sensitive to ionic strength changes as salt concentration increased. The salt dependence of A_2 is in general agreement with the changes observed in polyelectrolytes.[23,31] The behavior of polyelectrolytes in LIS conditions is quite complex, however, and a detailed discussion of the scattering of PBO in LIS solvents is outside the scope of this publication.[32]

In HIS solvents, A_2 showed some variability from sample to sample, but they were in the neighborhood of $A_2 \approx$ 0.06–0.03 cm^3 mol g^{-2}, generally decreasing as M_w increased. Such behavior has also been observed for poly(γ-benzyl α,L-glutamate).[29]

Assuming rodlike behavior, the effective rod–rod hard core repulsion diameter, d_H, is given by[33]

$$d_H = \frac{A_2}{\pi N_A}(M/L)^2 \tag{23}$$

The values of A_2 in Table II correspond to effective hard core molecular exclusion diameters between $d_H \sim 2.4$ and 4.7 nm.

This result can be compared with the effective electrostatic diameter of a charged cylinder given by Odijk's theoretical expression:[34]

$$d_H \approx d_0 + \kappa^{-1}\left[\ln\left(\frac{4\pi B_l}{b^2\kappa}\right) + 0.077\right] \tag{24}$$

where $d_0 \approx 0.5$–0.6 nm is the diameter of the uncharged rod, b is the distance between charges along the chain, κ^{-1} is the Debye screening length (in cm)

$$\kappa^{-1} = (8\pi N_A B_l I/1000)^{-1/2} \tag{25}$$

and

$$B_l = \frac{e^2}{D_e kT} \tag{26}$$

is the so-called Bjerrum length (in cm). D_e is the dielectric constant of the medium, and I is the ionic strength

$$I = (1/2)\sum m_i z_i^2 \tag{27}$$

where m_i is the molar concentration of solute with charge Z_i. The sum in eq 27 extends over all small ions, including those arising from added salts, the counterions created by the added polymer, and the acid self-dissociation:

$$2A = A^- + AH^+ \qquad K_\alpha = m_{A^-}m_{AH^+} \approx 1.2 \times 10^{-5} \tag{28}$$

The ionic strength in salt-free conditions is approximately $I \approx 3.5 \times 10^{-3}$ M, and the addition of 0.1 M monovalent salts such as NaMSA can be approximated by $I \approx 0.1$ M. This results in $\kappa^{-1} \approx 6$ nm in salt-free conditions, and $\kappa^{-1} \sim 0.98$–1.13 nm with 0.1 M NaMSA (assuming $D_e \approx 90$–120, or $B_l \approx 0.56$ nm).

Assuming two charges per repeat unit (b = 0.6 nm), the electrostatic rod–rod hard core repulsion diameter of *cis*-PBO (eq 24) becomes

$$d_H \text{ (nm)} \approx 0.5 \text{ nm} + \kappa^{-1}[\ln(19.5\kappa^{-1}) + 0.077] \tag{29}$$

At 0.1 M NaMSA, this expression results in $d_H \approx 3.5$ nm, in excellent agreement with the values estimated from A_2. In qualitative agreement with eq 23, A_2 increases with decreasing ionic strength, but it becomes difficult to estimate d_H because of the curvature in the plots (Figure 2). In the salt-free condition limit, eq 24 estimates $d_H \approx$ 29 nm, a remarkably long range exclusion diameter.

(E) Intrinsic Viscosity Dependence on Salt Concentration. If *cis*-PBO in MSA is a semiflexible polyelectrolyte chain, the stiffness of the backbone should decrease as ionic strength increases as a result of increasing charge screening along the backbone. The viscosity trends of Figure 1 and the strong viscosity concentration dependence of LIS solutions relative to the HIS solutions above their entanglement concentrations (Figure 3b) are consistent with this hypothesis.

The semistiff polyelectrolyte model, furthermore, can be tested quantitatively for the case of the $[\eta]$ dependence on salt concentration. Polyelectrolyte theories assume that total persistence length Q_t can be expressed as[35]

$$Q_t + Q_i + Q_e \tag{30}$$

where Q_i is the "intrinsic" component, dependent only on local backbone structure, and Q_e is the electrostatic contribution which results from charge repulsions along the backbone. A simple model for the electrostatic contribution is given by

$$Q_e = \frac{B_l}{4b^2\kappa^2} \tag{31}$$

where $b \approx 0.6$ nm is the effective distance between backbone charges. This value assumes that there are only two effective charges on each repeat unit. The number of charges was determined by conductimetry,[36] and it is also close to the theoretical charge density limit (equal to $B_l \approx 0.56$ nm assuming $D_e \approx 100$) of Manning's counterion condensation model.[37]

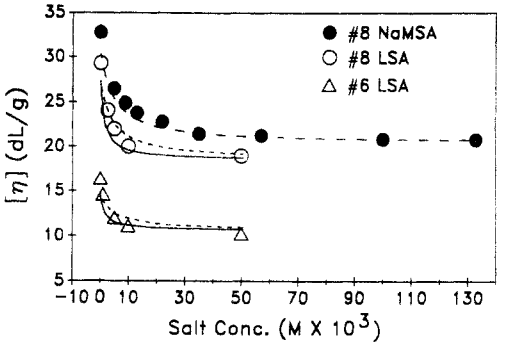

Figure 15. Polyelectrolyte model predictions for the dependence of $[\eta]$ on salt addition. The data correspond to sample 8 with NaMSA (filled circles) and LSA (open circles) and to sample 6 with LSA (open triangles). The curves were calculated using the Yamakawa–Fujii wormlike chain equations, assuming polyelectrolyte behavior (eq 32) with $Q_i = 19$ nm. The solid lines of the samples with LSA were calculated assuming SO_4^{2-}, and the broken lines assumed the formation of SO_4H^-.

To estimate the contribution Q_e under nearly salt-free conditions, the value of I should be known quite accurately. For a monovalent salt with common ion, such as NaMSA, this is given by[36]

$$I = (1/2)\{m_1 + m_{aH^+} + m_{A^-}\} \tag{32}$$

$$m_{AH^+} = -(1/2)(xm_p + m_1) + \left\{\left(\frac{xm_p + m_1}{2}\right)^2 + k_\alpha\right\}^{1/2} \tag{33}$$

where m_1 is the salt molar concentration, m_p is the repeat unit molar concentration, $x = 2$ is the degree of protonation, and $m_{A^-} = K/m_{AH^+}$ (see eqs 27 and 28).

Figure 15 compares the data of Figure 1 with the theoretical curves obtained using the Yamakawa and Fujii expressions with Q_t as functions of salt concentrations. The molecular parameters used to fit the data are $Q_i \approx 19$ nm and chain diameter $d = 0.6$ nm. The fit is very good for sample 8 with NaMSA assuming $M = 82.6$K (in very close agreement with the MH(G) results, $M_w = 82$K, $M_\eta \approx 81$K). For the case of LSA the ionic strength increases more rapidly with salt concentration, but there are two possible degrees of ionization: SO_4^{2-} or SO_4H^-. The solid curves in Figure 15 were calculated assuming the former case, and the short dashed curves correspond to the latter. The data of sample 8 with LSA were fitted assuming $M = 78.4$K (this value is slightly lower than for the NaMSA case), and the data of sample 6 were fitted with $M = 40.7$K. Both values are in very good agreement with the MH(G) relationship obtained in HIS solvent ($M_w = 38$K and $M_\eta \approx 38.7$K for sample 6). The polyelectrolyte semistiff model appears to be quite successful in reproducing the intrinsic viscosity changes of *cis*-PBO with the additions of two different salts and for two molecular weights. The agreement with the experimental values is very good for almost the entire range of ionic strengths of the experiment. According to this interpretation, the persistence length of *cis*-PBO changes from $Q_t \sim 32$ nm (LIS) to $Q_t \sim 19$–20 nm in HIS conditions.

The viscosity "plateau values" reached at 0.1 M NaMSA and 0.05 M LSA in Figure 15 were identical (within experimental error) to the viscosities of HIS solutions of the same polymers prepared *directly* from salted solvents (Table I). This indicates that the hypothetical degree of aggregation in solutions initially prepared in LIS conditions and later salted does not differ from those in which the solvent was initially a HIS one. We found no evidence that HIS solvents might be less effective in dissolving the polymer than LIS ones.

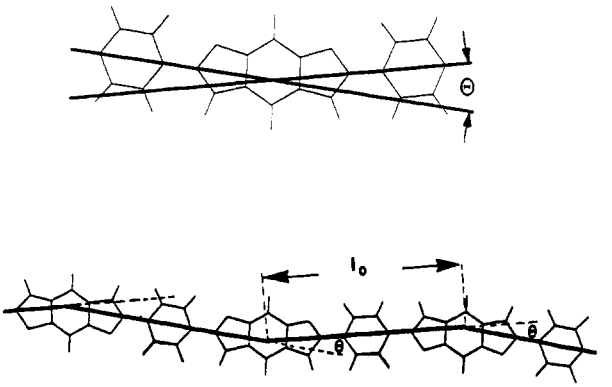

Figure 16. Top: Shape of the protonated *cis*-PBO model compound according to the Hartree–Fock *ab initio* molecular orbital calculation HF/3-21G. The heterocycle shows a "kidney-bean" shape which results in $\Theta \approx 14.7°$ deviation from linearity. For the unprotonated case, the distortion is less pronounced, and $\Theta \approx 9.7°$. Bottom: Simple virtual bond model of protonated *cis*-PBO in the absence of bond bending. All the virtual bonds are shown in the *trans* configuration ($\phi = 0$). The phenylene cycles are approximately linear, and the C–C bonds between the two cycles have nearly twofold rotational symmetry around ϕ. The angle between virtual bonds is $\Theta \approx 14.7°$. The persistence length of this model is $Q \approx 34$–37 nm without bond bending, and approximately $Q \approx 23$–30 nm assuming thermal bond bending. The unprotonated model predicts $Q \approx 84$ nm.

Figure 15 shows a small but noticeable difference between the data of samples 8 with MSA (filled circles) and 8 with LSA (open circles). Since this difference originates with the salt-free solutions ($[\eta] = 33$ and 29.5 dL/g, respectively), it is presumably caused by errors in solution preparation or by slight ionic strength differences in the solvents.

The agreement between model predictions and experimental results in Figure 15 appears to "break down" as the salt-free conditions are approached, where the data become considerably higher than the theoretical values (sample 8, no salts, measured $[\eta] = 33$ dL/g, but the model estimates $[\eta] = 29$ dL/g). This suggests that the viscosity behavior in this limit probably involves intermolecular interactions in addition to chain stiffening. Such interactions might also be responsible for the strong decrease in scattering intensity (Figure 2), the unusual dynamic light scattering behavior of this polymer in LIS solutions,[31,32] and the anomalous behavior of the solution viscosity at very low polymer concentrations in salt-free solutions (Figure 4).

Discussion

The wormlike chain model with chain stiffness in the neighborhood of $Q = 19$–25 nm is in excellent agreement with the apparent molecular characteristics of *cis*-PBO obtained by light scattering and intrinsic viscosity.

The possibility that *cis*-PBO might not be as rodlike as previously assumed is supported by recent molecular orbital (MO) calculations. *Ab initio* MO[38,39] (HF/3-21G) and semiempirical MO (AM1) calculations show that the *diprotonated* repeat unit of *cis*-PBO has considerable "kidney bean" shape deviation from linearity with a net deviation of $\Theta \approx 14.7$–15.1° from collinearity (Figure 16 (top)). This shape is the result of the significant differences in bond lengths and angles between the pair of C–NH–C bonds and the pair of C–O–C in the *cis* configuration. Assuming a simple virtual bond model[39] and "two-state" rotational isomerism, as indicated in Figure 16 (bottom), one obtains $Q \approx 34$–37 nm. If thermal fluctuations on

bond angles are also considered,[39] the estimated persistence length is reduced to approximately $Q \approx 23$–30 nm, in very good agreement with the experiments. Note: Figure 16 (bottom), with virtual bonds in the *trans* configuration, was also used to estimate the effective length of the repeat unit ($L_0\langle\cos(\Theta/2)\rangle$) for the YF shift factors ($M_L \approx 196$–203 Da nm^{-1}).

In the *unprotonated* (neutral) state, on the other hand, the *ab initio* calculations[38,39] predict less bending ($\Theta \approx 9.7°$ and $Q \approx 80$ nm without angle fluctuations), suggesting that the chain is statistically much more straight in the solid state than in solution.

A different calculation[40] (molecular dynamics) carried out by Farmer and co-workers also suggests relatively low persistence length for *cis*-PBO: $Q = 32.5$ nm. The deviations from rodlike shape were attributed primarily to bendings of the plane of the molecule and not to the "kidney bean" shape distortion mentioned above. Another approach[41] by Zhang and Mattice used rotational isomeric state calculations to obtain $Q \approx 65$ nm for *cis*-PBO and $Q \approx 32$ nm for *trans*-PBT. These authors assumed much less *cis*-PBO bending and they apparently ignored the *cis* and *trans* symmetry constraints on the conformation of the corresponding heterocycles.[39] The molecular model calculations, therefore, do not rule out the possibility of semiflexible behavior for PBO, but there are serious discrepancies between methods[39–41] as well as between some of these methods[40,41] and experiments.

The semistiff chain model presented in this publication provides an alternative model to rod–rod aggregation as a way to explain the apparent deviations of *cis*-PBO from ideal rodlike behavior in HIS conditions and the changes of solution behavior with ionic strength. The results, however, do not rule out completely the aggregation hypothesis. Aggregation (parallel generation of dimers, trimers, etc.) is also capable of explaining many of the phenomena presented in this paper, albeit in a more complex[42] and possibly less quantitative fashion than the semistiff model. The aggregation hypothesis is very difficult to either verify or reject since it assumes that the actual molar solute concentrations are not well defined.

The semiflexible polyelectrolyte model is in agreement with several important aspects of PBO behavior in moderately low and high ionic strength conditions. This single-chain model, however, is not capable of explaining many aspects of the very low ionic strength behavior, such as the dynamic light scattering[31,32] and the salt-free limit of the intrinsic viscosity. It appears that the LIS behavior actually may be affected by large ordered structures with some resemblance to polymer colloids[43] and the "extraordinary regime" observed in biopolymers under low ionic strengths.[44] These hypothetical extended transient ordered domains, however, are postulated for LIS conditions, where the electrostatic diameter becomes of the order of tens of nanometers, and are not aggregates in the same sense as the hypothetical HIS clusters mentioned above and in the Introduction.

Finally, it should be mentioned that the *cis*-PBO backbone stiffness in solution might not be the same as in the solid state. In addition to the crystallization energy which introduces order and suppresses bond angle fluctuations, the backbone of PBO probably becomes more than threefold stiffer when it becomes neutralized, as suggested by the considerable reduction in the *ab initio* MO bending angle estimates (from $\Theta \approx 15°$ to $\Theta \approx 9.7°$). This suggests that the deprotonation of the chain might be accompanied by considerale conformational changes. Similar changes probably also occur during the dissolution (and coagulation) of other high-performance polymers, such as aramids, but these transitions and their effect on solid-state polymer morphology and properties have not received, in general, sufficient attention.

Summary

The wormlike chain polyelectrolyte model with persistence length between $Q = 32$ nm (LIS) and $Q = 19$–20 nm (HIS) is in excellent agreement with the static light scattering and the intrinsic viscosity behavior of *cis*-PBO in MSA. The HIS persistence length ($Q \approx 19$–25 nm) accounts for the deviation of the Mark–Houwink (G) relationship from ideal rod behavior, the change of radius of gyration with molecular length in HIS, and the change of intrinsic viscosity with ionic strength. The polydispersity ratio $M_w/M_n \approx 1.6$–1.97 was determined from four samples with defined stoichiometry (the value is closer to 2 for the end-labeled samples) and suggests that the measured molecular weights correspond to individual molecules, not aggregates.

The intrinsic viscosity dependence on ionic strength is well accounted for by the semistiff polyelectrolyte model (with persistence length $Q \approx 19$ nm), at least for two samples of considerably different molecular weights (82K and 38K) and for two different salts (NaMSA and LSA).

The hypothesis that *cis*-PBO in solution probably deviates considerably from an ideal rolike shape is in qualitative agreement with recent molecular oribtal calculations. Further research in this area is needed in light of the strong discrepancies between the predictions of the various theoretical approaches.

The interpretation of the solution behavior in terms of a semistiff polyelectrolyte chain model is not the *only* explanation for the solution behavior of *cis*-PBO. The phenomena described in this publication can also be interpreted in terms of small clusters of parallel rods. The semistiff chain model, however, deserves serious consideration since it provides a simpler explanation for a broad number of experiments and it can be checked quantitatively.

The high degree of alignment and extraordinary physical properties of *cis*-PBO fibers suggest that these characteristics are less dependent on the solution state of the polymers than previously thought (assuming semistiff behavior). *Ab initio* MO calculations suggest that the unprotonated chains are more "rodlike" than their solvated counterparts. As long as the fiber spinning conditions provide sufficient chain alignment, the fiber tensile properties are ultimately determined by their characteristics in the solid state, such as crystallinity, molecular geometry, and molecular weight.

Acknowledgment. The authors thank Brian Barron and Drs. Ying So, Charlie Hotz, and Pete Pierini for providing polymer samples and Drs. Steve Martin, Lu Ho Tung, Steve Lefkowitz, Skip Rochefort, and Nelson Beck for useful comments and discussions. The authors also express appreciation to Bruno Zimm, Robert Cook, and Mark Mansfield for helpful suggestions regarding the rotational isomeric behavior of PBO.

Appendix A

The Yamakawa–Fujii (YF) expressions[20] were computed as follows.

(A) For $L > 5.4Q$

$$[\eta]\ (\mathrm{dL/g}) = \frac{\phi(y)y^{3/2}(2Q)^3}{M} \times 10^{-26} \qquad \text{(A-1)}$$

$$\phi(y) = 2.87 \times 10^{23}(1 - \sum_{j=1}^{4} C(\chi)_j y^{-j/2})^{-1} \quad \text{(A-2)}$$

where the functions $C_j(\chi)$ are defined in YF's paper, the reduced diameter and chain lengths are given by $\chi = d/(2Q)$ and $y = (M/M_L)/(2Q)$, respectively, M is the molecular weight, and M_L is the "shift factor". In expressions A-1 and A-2, the lengths are in angstroms.

(B) For $L < 5.4Q$

$$[\eta]\ (\mathrm{dL/g}) = [\eta]_{rr}\left(\frac{G(y)(2Q)^3 \times 10^{-26}}{1 + \sum_j A_j[\ln(\chi/y)]^{-1}}\right) \quad \text{(A-3)}$$

where the function G is given by

$$G(y) = \left(\frac{3}{2y^4}\right)[e^{-2y} - 1 + 2y - 2Y^2 + (4/3)y^3] \quad \text{(A-4)}$$

and the "rigid rod" factor $[\eta]_{rr}$ is given by eq 19. The coefficients in the above sum are $A_1 = 1.839$, $A_2 = 8.24$, $A_3 = 32.862$, and $A_4 = 41.1045$.

The values corresponding to the overlapping regions $L \approx 5Q$ were interpolated by simple inspection from computed tables of values from eqs A-1 and A-3.

Appendix B

The "s"-average molecular weight is given by

$$M_s = (m_w^{-1}\sum_i w_i M_i^{1+p})^{1/p} \quad \text{(B-1)}$$

where $1 \le p \le 2$. According to Flory's most probable distribution,[25,28]

$$M_w = \frac{1+\gamma}{1-\gamma} \quad \text{(B-2)}$$

and

$$M_s(p) = \left[\frac{(1-\gamma)^3}{1+\gamma}B(p)\right]^{1/p} \quad \text{(B-3)}$$

where

$$B(p) = \sum_1^\infty \gamma^{i-1} i^{2+p} \quad \text{(B-4)}$$

and γ is the extent of reaction ($M_w \to \infty, \gamma = 1$). Equations B-3 and B-4 were computed by direct summation over 3000 terms for $\gamma = 0.99$ (the sum is slowly convergent) as a function of p. The result is the linear relationship

$$M_s/M_w = 1.269 + 0.232p, \quad 1 \le p \le 2 \quad \text{(B-5)}$$

In the coil limit ($p = 1$) the eq B-5 estimates $M_s/M_w = 1.501$, and for rigid rods ($p = 2$) $M_s/M_w = 1.733$, both values in excellent agreement with the analytical expressions (3/2 and $3^{1/2}$, respectively). The relationship in eq B-5 is a numerical approximation which needs to be verified analytically.

The value of p was estimated (as a first approximation) as

$$p(M) \approx \frac{\partial \log(R_g^2)}{\partial \log(M)} \quad \text{(B-6)}$$

This expression may be computed either from a quadratic least-squares data fitting or from the wormlike chain model (eq 9) assuming $Q \approx 20$–25 nm.

References and Notes

(1) *The Materials Science and Engineering of Rigid-Rod Polymers*; Adams, W. W., Eby, R. K., McLemore, D. E., Eds.; Symposium Proceedings; Materials Research Society: Pittsburgh, PA, 1989; Vol. 134.
(2) Wong, C. P.; Ohnuma, H.; Berry, G. C. *J. Polym. Sci., Polym. Symp.* **1978**, *65*, 173.
(3) Choe, E. W.; Kim, S. N. *Macromolecules* **1981**, *14*, 920.
(4) (a) Gregory, T.; Hurtig, C. W.; Ledbetter, H. D.; Quackenbush, K. J.; Rosenberg, S. U.S. Patent 5 089 591, 1992. (b) Wolf, J. F. In *Encyclopedia of Polymer Science and Engineering*, 2nd ed.; Mark, H. F., et al., Eds.; Wiley: New York, 1988; Vol. 11, p 601.
(5) Metzger Cotts, P. C. Ph.D. Thesis, Carnegie Mellon University, 1980.
(6) Metzger Cotts, P. C.; Berry, G. C. *J. Polym. Sci., Polym. Phys. Ed.* **1983**, *21*, 1255.
(7) Berry, G. C. In *Contemporary Topics in Polymer Science*; Pearce, E. M., Ed.; Plenum: New York, 1977; Vol. 2, pp 55–96.
(8) Furukawa, R.; Berry, G. C. *Pure Appl. Chem.* **1985**, *57*, 913.
(9) Welsh, J. W.; Mark, J. E. *Polym. Eng. Sci.* **1983**, *23*, 140.
(10) Doty, P.; Bradbury, J. H.; Holtzer, A. M. *J. Am. Chem. Soc.* **1956**, *78*, 947.
(11) Wessling, R. A.; Mark, J. E.; Hamori, E.; Hughes, R. E. *J. Phys. Chem.* **1966**, *70*, 1903.
(12) Nagai, K. *Polym. J.* **1972**, *3*, 67.
(13) Brelsford, G. L.; Krigbaum, W. R. In *Liquid Crystallinity in Polymers*; Cifferri, A., Ed.; VCH: New York, 1991; Chapter 2.
(14) Berry, G. C. *J. Chem. Phys.* **1966**, *44*, 4550.
(15) Benoit, H.; Doty, P. *J. Phys. Chem.* **1953**, *57*, 958.
(16) Arpin, M.; Strazielle, C. *Makromol. Chem.* **1976**, *177*, 581; *Polymer* **1985**, *26*, 1401.
(17) Roitman, D. B.; McAlister, J.; Oaks, F. L. *J. Chem. Eng. Data*, in press.
(18) Hu, N.; Amis, E.; Roitman, D. B.; Wessling, R. A., unpublished data.
(19) Huglin, M. B. In *Topics in Current Chemistry*; Boschke, F. L., Ed.; Springer-Verlag: Berlin, 1978; Vol. 77, p 143.
(20) Yamakawa, H.; Fujii, M. *Macromolecules* **1974**, *7*, 128.
(21) Fartini, A. V.; Lenhert, P. G.; Resch, T. J.; Adams, W. W. In *The Materials Science and Engineering of Rigid-Rod Polymers*; Adams, W. W., Eby, R. K., McLemore, D. E., Eds.; Symposium Proceedings; Materials Research Society: Pittsburgh, PA, 1989; Vol. 134, p 431.
(22) Billmeyer, F. W., Jr. *J. Polym. Sci.* **1949**, *4*, 83.
(23) Kaye, W.; McDaniel, J. B. *Appl. Opt.* **1974**, *13*, 1934.
(24) Doi, M.; Edwards, S. F. *The Theory of Polymer Dynamics*; Oxford University Press: Oxford, 1986; p 312.
(25) Flory, P. *Principles of Polymer Chemistry*; Cornell University Press: Ithaca, NY, 1953; Chapter 3.
(26) So, Y. H., unpublished results.
(27) Schaefgen, J. R.; Flory, P. J. *J. Am. Chem. Soc.* **1948**, *70*, 2709.
(28) Kratochvil, P. In *Light Scattering from Polymer Solutions*; Huglin, M. B., Ed.; Academic Press: New York, 1972; Chapter 7.
(29) DeLong, M. L.; Russo, P. S. *Macromolecules* **1991**, *24*, 6139.
(30) Bhaumik, D.; Jaffe, H. H.; Mark, J. E. *Macromolecules* **1981**, *14*, 1125.
(31) Ferrari, M. E.; Bloomfield, V. A. *Macromolecules* **1992**, *25*, 5266.
(32) Tracy, M. Ph.D. Thesis, Stanford University, 1992.
(33) Zimm, B. H. *J. Chem. Phys.* **1946**, *14*, 164.
(34) Odijk, T. *Macromolecules* **1986**, *19*, 2313.
(35) Skolnick, J.; Fixman, M. *Macromolecules* **1977**, *10*, 944.
(36) Roitman, D. B.; McAlister, J.; McAdon, M.; Martin, E.; Wessling, R. A., submitted to *J. Polym. Sci., Polym. Phys. Ed.*
(37) Manning, G. R. *Q. Rev. Biophys.* **1978**, *11*, 179.
(38) Shaffer, A. A.; Wierschke, S. G. *J. Comput. Chem.* **1992**, *14*, 75.
(39) Roitman, D. B.; McAdon, M. *Macromolecules*, in press.
(40) Farmer, L. B.; Chapman, B. R.; Dudis, D. S.; Adams, W. W. *Polymer* **1993**, *34*, 1588.
(41) Zhang, R.; Mattice, W. L. *Macromolecules* **1992**, *25*, 4937.
(42) Schott, P. *Chem. Phys.* **1992**, *96*, 6083.
(43) Ise, N.; Matsuoka, H.; Ito, K. *Macromolecules* **1989**, *22*, 1.
(44) Lee, W. I.; Schurr, J. M. *J. Polym. Sci., Polym. Phys. Ed.* **1975**, *13*, 873.
(45) Adams, W. W.; Kumar, S.; Martin, D. C.; Shimamura, K. *Polym. Commun.* **1989**, *30*, 285.